Plasmonic Modes of Metallic Semishells in a Polymer Film

Jian Ye,[†,‡,*] Niels Verellen,[§,†,⊥] Willem Van Roy,[†] Liesbet Lagae,[†,∥] Guido Maes,[‡] Gustaaf Borghs,[†,∥] and Pol Van Dorpe[†]

[†]IMEC, Kapeldreef 75, Leuven, B-3001, Belgium, [‡]Chemistry Department, [§]INPAC-Institute for Nanoscale Physics and Chemistry, [⊥]ESAT-TELEMIC, and [∥]Physics Department, Katholieke Universiteit Leuven, Leuven, B-3001, Belgium

ARTICLE

ABSTRACT The symmetry-broken geometry and variation of metal composition of semishells induce new plasmonic properties. A system of separated metallic semishells embedded in a poly(dimethylsiloxane) polymer film provides an ideal platform to investigate the localized surface plasmon resonance modes of semishells. We demonstrate experimentally that silver, gold, copper, and aluminum semishells can offer distinct plasmonic responses due to the wide range of their material parameters. Numerical calculations combined with the plasmon hybridization theory render us a clear understanding and assignment of the plasmonic modes of the semishells.

KEYWORDS: semishell · nanoshell · plasmon · finite difference time domain · poly(dimethylsiloxane) · antibonding mode

Metallic semishells, typically composed of a dielectric core and an incomplete ultrathin metal shell, induce a number of new optical, magnetic, and catalytic properties.[1−4] For example, Srivastava *et al*. have reported Co semishells, prepared by vacuum assisted infiltration of precursors inside the colloidal templates, which have an enhanced coercivity in comparison to Co nanoparticles in the same size range.[3] Liu *et al*. have shown ordered arrays of Pt semishells from silica sphere templating and nanocrystal-seeded electroless plating, and their high ratio of surface area to volume shows promising catalytic properties.[4] All of these unconventional properties of semishells have motivated more research efforts in developing new methods of asymmetrical semishells fabrication. Au and Ag nanostructures are known to have interesting optical properties such as localized surface plasmon resonances (LSPR) which are collective oscillations of the conduction electrons excited by incident radiation. Previously, we have reported on a simple procedure involving an ion milling technique to fabricate Au semishells.[5] Those Au semishells possess favorable features for surface-enhanced Raman spectroscopy (SERS): an interparticle distance independent enhanced localized electromagnetic field, a precise control of the symmetry-broken geometry, and the uniform upward orientation of the created nanoapertures. Recently, more plasmonic (Au, Ag, and Al) semishells with highly tunable optical properties including nanocups, nanocaps, nanobowls, and nanocrescents have been fabricated. Their plasmonic resonances strongly depend on the fractional height of the shells and the angle and the polarization of the incident light.[6−12] They have also suggested and demonstrated as interesting substrates for SERS-based molecular detection.[6,13] By contrast, we would like to understand the nature of the plasmonic modes of the individual semishells, since they are suitable nanostructures to investigate plasmon hybridization between the inner and outer shell surface.[14] However, most of the work cited above has been focusing on semishells formed by deposition of continuous metal films on contiguous polystyrene (PS) arrays. The obtained contiguous semishells are to some extent difficult and complex systems to analyze the plasmonic properties of individual semishells since both delocalized Bragg plasmons and localized Mie plasmons are involved.[12,15] Moreover, direct metal deposition on PS arrays also creates extra metallic truncated tetrahedral nanoparticles on the substrate,[7,16,17] which give their own optical responses and complicate the accurate analysis of the plasmonic response from the individual semishells.

In the present article, we report on the fabrication and the optical properties of semishells, consisting of a PS core and an arbitrary metal shell, embedded in a poly(dimethylsiloxane) (PDMS) polymer film. The structure of metallic semishells in PDMS is an interesting platform to investigate the

*Address correspondence to Jian.Ye@imec.be.

Received for review October 29, 2009 and accepted January 27, 2010.

Published online February 4, 2010. 10.1021/nn901519p

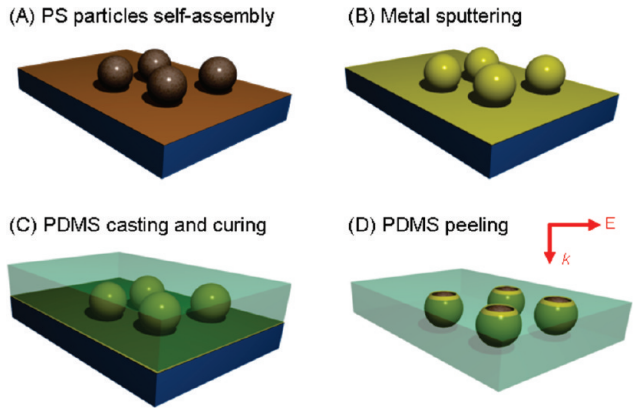

Figure 1. Experimental procedure for fabricating metallic semishell films.

plasmonic properties of individual semishells due to the absence of semishell aggregation, a tunable composition and thickness of the metal layer, and a well-controlled orientation of the semishells. The fabrication is based on metal sputtering on a *submonolayer* of PS particles on the substrate, followed by a curing and peeling of a casted PDMS film on the metallic nanostructures. Further details are provided in the Methods section. Notably, the preparation method is suitable for noble metals such as Au and Ag but also for less commonly used plasmonic metals like Cu, Al, and Pt, and may be applied to fabricate more complex symmetry-broken nanostructures consisting of complex multilayer shells with a varying composition. This method allows us to minimize the influence on the plasmonic properties from the roughness of the metal shell using chemical plating,[18] but it may be limited for an ultrathin film (*e.g.*, $<$10 nm) because the ultrathin film may produce a porous structure. The PDMS matrix may also reduce the oxidation of some metals, such as Ag, Cu, and Al, which provides more accurate optical measurements. Different techniques including scanning electron microscopy (SEM) and atomic force microscopy (AFM) have been used to characterize the semishell polymer film structures. Plasmonic properties of semishells from various shell thicknesses and metal composition are investigated experimentally and theoretically, showing highly tunable plasmon resonances ranging from the ultraviolet (UV) to the near-infrared (NIR) region. Finite difference time domain (FDTD) calculations are performed to analyze the electric field profiles and surface charge distributions in order to fully understand the plasmonic modes of the semishells. The plasmonic properties of various metallic semishells are well explained by the plasmon hybridization theory and the different frequencies where interband transitions occur for different metals. To illustrate this, we clearly demonstrate both experimentally and theoretically the occurrence of the antibonding dipolar resonance in the Ag semishells. The antibonding resonance is a clear prediction of the hybridization theory but has been difficult to observe due to its energetic overlap with the interband transitions in most metals. Additionally, enhanced electric fields on the top aperture of the semishells are found in the dipolar and quadrupolar modes.

RESULTS AND DISCUSSION

Figure 1 describes the standard procedure to fabricate metallic semishells in a polymer film. Typically, 100 nm PS particles form a submonolayer on a polydiallyldimethylammonium (PDDA)-functionalized substrate as a template, followed by sputtering a metal (Au, Ag, Cu, or Al) layer of 10−30 nm thickness on top. The substrate functionalization with PDDA molecules is crucial during the self-assembly of PS particles. The electrostatic repulsive force between PS particles and the attractive force between PDDA molecules and PS particles allow the formation of a uniform submonolayer on the substrate. Figure 2A shows a SEM image of a self-assembled submonolayer of 100 nm PS particles, indicating that all PS particles are uniformly distributed and isolated with an interparticle distance of ~200 nm without an ordered lattice structure. After 30 nm Au layer deposition on the PS particles, almost no morphology change was observed (Figure 2B). The side-view SEM image in the inset of Figure 2B indicates that PS particles are entirely covered by a continuous Au film except the parts that contact the substrate. This local discontinuity of the Au film makes it possible to separate the Au layer on the PS particles from the interparticle Au layer by the peeling process. Next, PDMS mixed with the curing agent was directly casted on the substrate and cured at 50 °C in vacuum overnight. Finally, the PDMS films containing embedded semishells were peeled off the substrate. The obtained semishells are embedded in the polymer film while the remaining flat metal film is still attached to the substrate. Figure 2C

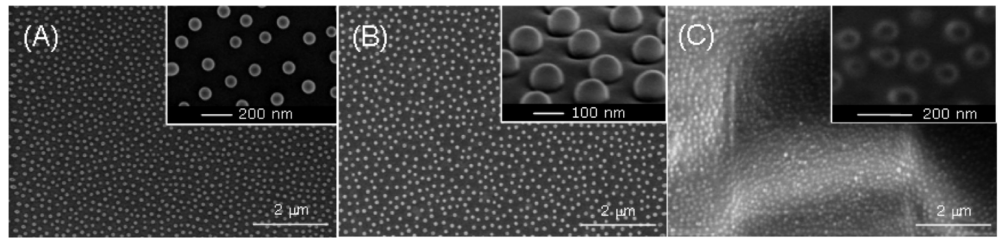

Figure 2. SEM images at different steps of the Au semishell film fabrication. (A) Self-assembled submonolayer of 100 nm PS particles, (B) followed by 30 nm Au sputtering, and (C) PDMS film peeling off. All insets are corresponding high magnification SEM images.

displays a SEM image of uniformly distributed Au semishells embedded in a PDMS matrix taken from the side of the shells' apertures. A closer examination presented in the inset of Figure 2C clearly shows a 40−50 nm sized nanoaperture on the top of each semishell and all semishells are isolated from each other with a distance of 50−100 nm.

AFM measurements were performed to investigate the surface morphology of a Au semishell film in more detail. Figure 3A shows the AFM topographic image (1 μm × 1 μm) of the 30 nm thick semishells embedded in PDMS that are shown in Figure 2C. For the three typical semishells indicated in Figure 3A a line scan is shown in Figure 3B. We can clearly see that most of the semishells are individually isolated with an aperture of ~50 nm in average size on the top, which is quite close to the previous SEM result. More interestingly, it is observed from Figure 3B that all semishells are partially embedded in PDMS with a 10−20 nm distance above the PDMS surface. The top aperture structures are completely open to the surrounding medium. This topography possibly is explained by a combined influence of a surface tension effect during the filling process and a shrinking effect during the curing process of the PDMS polymer. This morphology is potentially useful for SERS application where biomolecules may be adsorbed on the electromagnetic field enhanced regions. Because of the incomplete peeling of the particles off the substrate, a small quantity of voids between the semishells may exist (Figure S1 in Supporting Information).

For the fabrication of metallic semishells, there are a number of important processing parameters to be optimized. First, extra care has to be taken during the drying procedure of the PS submonolayer to prevent particle aggregation caused by capillary forces associated with water evaporation. Second, the adhesion of the polymer to the gold surface is closely related to the ratio of the PDMS prepolymer to the curing agent. For example, less than 50% of the particles was peeled off the substrate (Figure S2A in the Supporting Information) because of insufficient adhesion between the polymer and the gold surface if a ratio of 10:1 (prepolymer: curing agent) was used, whereas, for a ratio of 5:1, too strong adhesion between the polymer and the gold surface caused the gold layer on the flat surface to be peeled off as well, and we can only see uncovered PS particles from the bottom side (in Figure S2B in Supporting Information). To circumvent this issue, a 10 nm Ti layer was deposited on the substrate prior to the fabrication as an adhesion layer to increase the adhesion of the Au film to the substrate. Therefore, we can easily peel off the particles while keeping the Au film on the substrate.

The metallic semishells in PDMS provide a favorable platform to investigate the plasmonic properties of nonaggregated semishells. Figure 4 compares the experimental and calculated extinction spectra of Ag, Au,

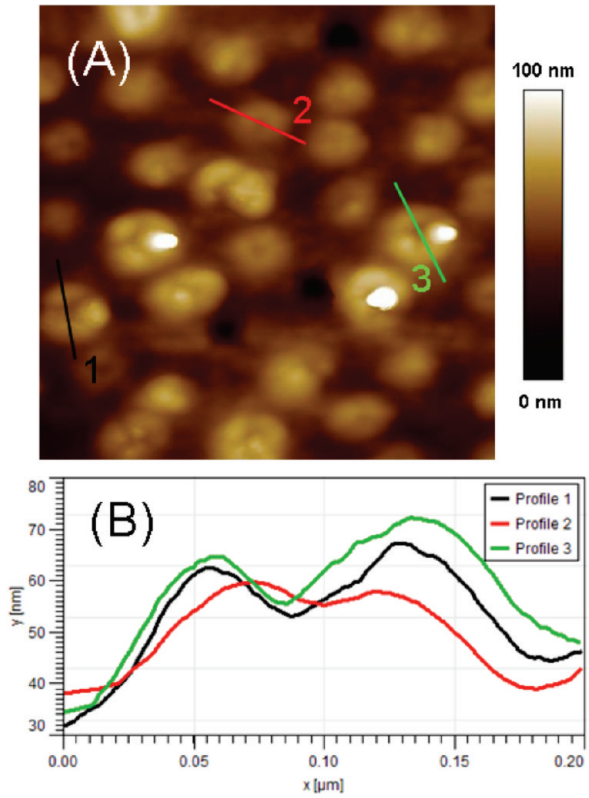

Figure 3. (A) AFM topographic image (1 μm × 1 μm) of a Au semishell film. (B) Representative line scans of the semishells indicated in panel A.

Cu, and Al semishells with different shell thicknesses. Different plasmonic behaviors are observed for the different semishells (see different colors in the photographs of Ag, Au, Cu, and Al semishells in Figure 4). For the Ag semishells, the experimental extinction spectra always show multiple LSPR bands, for instance, at 793, 650, and 349 nm for 10 nm thick Ag semishells and at 639, 462, 412, and 341 nm for 30 nm thick Ag semishells (Figure 4A). The resonance bands at 793, 650, 639, 462, and 412 nm are assigned to the dipolar, quadrupolar, and even octupolar resonances of Ag semishells, which is consistent with previous reports.[11,12] However, there are few reports and discussions about the resonance bands near the UV region, such as 349 nm for 10 nm Ag semishells and 341 nm for 30 nm Ag semishells, which are possibly attributed to higher order modes or the dipole antibonding mode. We will return to this later on. For both the Au semishells of 10 and 30 nm in shell thickness, only two bands in the visible or NIR range are detected experimentally and there is no plasmonic band near the UV range (Figure 4B). The bands in the NIR and the visible range correspond to the dipolar and quadrupolar resonances of the Au semishells, respectively.[5,6] For the Cu semishells with different thicknesses, the dipolar resonance is observed while the quadrupolar resonance is dramatically damped and exhibits a rather weak spectral shoulder (Figure 4C).

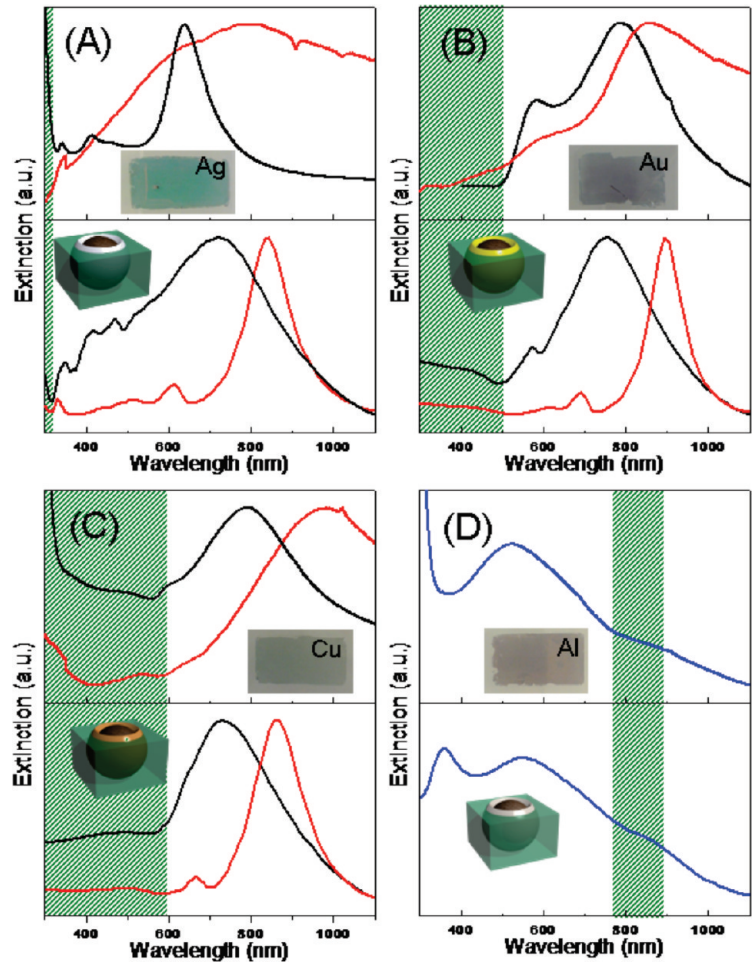

Figure 4. (Top) experimental and (bottom) calculated extinction spectra of (A) Ag, (B) Au, (C) Cu, and (D) Al semishells with various shell thickness (red, 10 nm; blue, 20 nm; and black, 30 nm) in a PDMS film. The insets are the corresponding (top) photographs and (bottom) schematics of the metallic semishells. The green shaded areas indicate the wavelength regions where interband transitions of the metals occur.

FDTD calculations are performed for individual 100 nm inner diameter semishells of different metals partially embedded in a PDMS matrix. Because the distance between the semishells in our fabricated samples is large enough to ignore the interparticle interaction, the calculation of individual semishells is a valid assumption. All calculated extinction spectra qualitatively reproduce the experimental spectra with respect to the number, position, and relative intensity of the resonance bands for the semishells of Ag, Au, and Cu with two different thicknesses (Figure 4A−C). Some global features are apparent: (1) decreasing the shell thickness results in a pronounced red shift of the plasmon bands; (2) the number of plasmon bands is different for Ag, Au, and Cu semishells of the same size. The former phenomenon is possibly explained by the plasmon hybridization theory, where the thinner shell thickness leads to a stronger plasmon interaction between the inner and outer shell surface and consequently a lower energy level of the resonance band.[14] The latter reduction of the number of plasmon bands can be understood by the fact that the electronic interband transitions occur at different energy regions for Ag, Au, and Cu. The spectral regions in Figure 4A−C where interband transitions occur are shaded in green.[19,20] The electronic transitions from the energetically deeper valence band into the conduction band form a steep absorption edge starting at the threshold frequency, above which all plasmon resonances are dramatically damped. This threshold energy for Ag is at ~3.8 eV (~326 nm), resulting in a minimal damping of plasmon resonances at short wavelengths.[19,20] Au has a lower energy onset of the interband transitions at ~2.5 eV (~500 nm), thus we may still observe the quadrupolar and dipolar modes of the Au semishells of 10 and 30 nm shell thickness.[19,20] The interband transition in Cu at even lower energy of ~2.1 eV (~590 nm) results in an apparent damping of the quadrupolar mode of the Cu semishells.[19,20] We have also found that the experimental plasmon bands are broadened compared to calculations for decreasing thickness of the shell. This can possibly be attributed to two effects: (1) an inhomogeneous or a porous metal shell formed on the PS core during the sputtering of 10 nm thick metal lay-

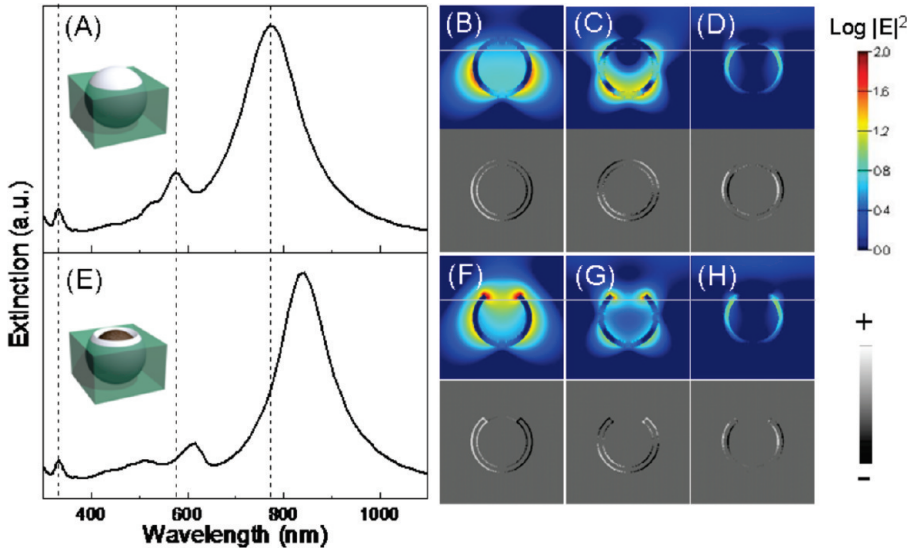

Figure 5. Calculated extinction spectra of a 10 nm thick (A) Ag nanoshell and (E) Ag semishell in a PDMS film, and their electric field (log|*E*|^2) profiles (top) and charge distribution (bottom) from horizontal cuts at the center of a Ag nanoshell at three on-resonance excitation wavelengths of (B) 770, (C) 575, and (D) 332 nm, and a Ag semishell at three on-resonance excitation wavelengths of (F) 843, (G) 615, and (H) 332 nm.

ers[21] and (2) a different extent of the oxidation of the metal. In an ensemble optical measurement, small structural differences may lead to a significantly broadened spectrum. Slight oxidation may also induce a dramatic change of the optical properties of Ag semishells, which explains the extremely broad spectrum of 10 nm Ag semishells compared to the other metals. Another notable spectral variation is the difference in the dipolar bandwidth between the experimental and calculated results for Ag semishells with a 30 nm shell thickness (Figure 4A). From our additional simulation results (data not shown), the theoretical extinction spectrum in air is more similar to the experimental spectrum in PDMS for the Ag semishells with a 30 nm shell with respect to the band's width and shape, suggesting that the Ag semishells are possibly less embedded in the PDMS matrix than other metallic semishells.

Unlike Ag, Au, and Cu, Al has a moderately strong interband transition in a narrow energy range of ~1.4 (~890 nm) − ~1.6 eV (~775 nm),[22,23] below and above which the interband activity is weak and Al behaves like a Drude metal.[24] Figure 4D shows the experimental and calculated extinction spectra of Al semishells with 20 nm shell thickness. We can see a strong dipolar plasmon band at ~550 nm in both spectra, which is at the higher energy side of and not damped by the interband transition of Al. The dipolar plasmon mode at 550 nm is elucidated by the electric field profile in Figure S3 in the Supporting Information. An additional feature of a spectral shoulder at ~870 nm is clearly observed, which is located within the interband transition range of Al. This feature has also been reported previously by Langhammer et al. for Al nanodisks.[24] It is not clear at present why we do not observe the quadrupolar mode (~360 nm) of the Al semishell in the experimental spectrum (Figure 4D) and further study is underway. An overview of all spectra of Ag, Au, Cu, and Al semishells tells us that the interband transitions of the metal can occur at the higher (e.g., Ag, Au, and Cu) or lower energy side of the dipolar plasmon band (e.g., Al), leading to remarkably different plasmonic mode damping behaviors of metallic semishells.

A large discrepancy among the extinction spectra of Ag, Au, and Cu semishells is the presence of the resonance band at 340−350 nm for Ag semishells while absent for Au and Cu. To further understand the plasmonic modes of Ag semishells, a comparison of calculated extinction spectra of 10 nm thick Ag nanoshells and Ag semishells and their corresponding electromagnetic field and charge distribution profiles are shown in Figure 5. Figure 5A displays three pronounced plasmon resonance bands of Ag nanoshells at 770, 575, and 332 nm. The former two bands are attributed to the dipolar and quadrupolar modes, which is confirmed by the electric field and surface charge profiles at 770 nm (Figure 5B) and 575 nm (Figure 5C). The field enhancement inside the metal of the Ag shell and the absence of the enhancement on the inner and outer surface of the shell (see Figure 5D) indicate an asymmetric distribution of the charges on the inner and outer surface, namely, an antibonding like mode for the plasmon band at 332 nm.[14,25−27] Although the surface charge profile in Figure 5D indicates as well the presence of multipolar modes, the antibonding mode dominates. It is easily understood that a multipolar mode is involved at a short wavelength since the diameter of the Ag semishell is close to half of the light wavelength at 332 nm. We therefore conclude that the resonance band at 332 nm is a mixture of a multipolar with the antibonding mode of the Ag semishell. Figure 5E

shows an extinction spectrum of a 10 nm thick Ag semishell with red-shifted dipolar and quadrupolar plasmon bands at 843 and 615 nm, respectively. These two modes are further elucidated by the electric field and surface charge profiles in Figure 5F,G, respectively. The red shift of the dipolar and quadrupolar bands can be explained by the plasmon hybridization of the nanoshell and the nanoaperture, resulting in a lower energy mode at a longer wavelength.[1,28] Additionally, a strong localized field enhancement at the top edges of the Ag semishell is observed compared to the Ag nanoshell at two on-resonance wavelengths, which provides interesting prospects for SERS application. It is interesting to find that the plasmon band of the semishell at 332 nm remains at the same position as the Ag nanoshell (Figure 5E). Removal of a small part on the top of the Ag nanoshell only affects the multipolar resonance and has almost no influence on the dominant antibonding mode, consequently resulting in no change of the position of the band. This is confirmed by the electric field and surface charge profile in Figure 5H as well. We have also calculated the extinction spectra of the nanoshell and the semishell for Au (Figure 6A) and Cu (Figure 6B). A comparison of these spectra indicates a common trend: removing the top of the nanoshell results in a red shift of the dipolar and quadrupolar resonance bands, which is consistent with the result for the Ag semishell in Figure 5. This is again due to the plasmon hybridization of the nanoshells and the nanoapertures. The electric field and surface charge profiles of a Au semishell at on-resonance wavelengths in Figure 6C,D additionally demonstrate the dipolar and quadrupolar modes.

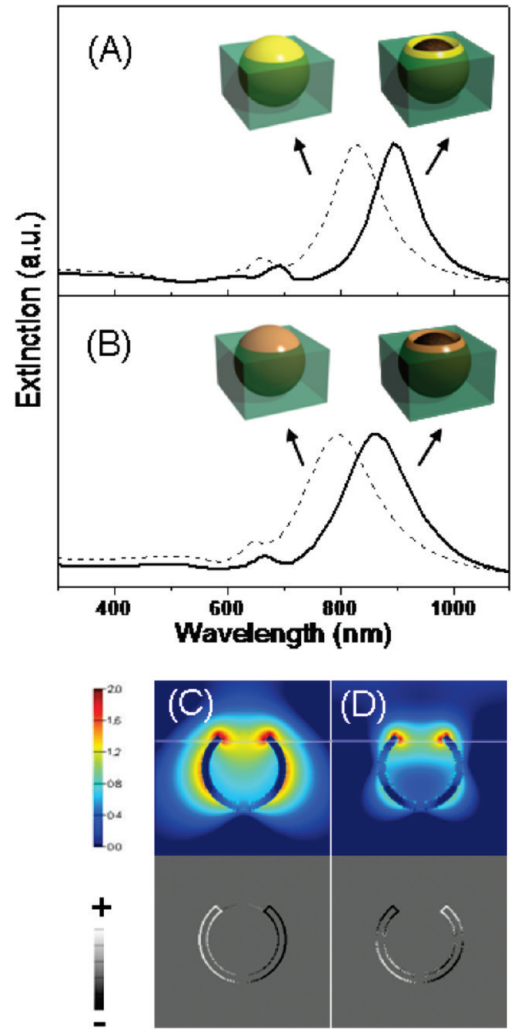

Figure 6. Calculated extinction spectra of a 10 nm thick (A) Au nanoshell (dashed line) and semishell (solid line) and (B) Cu nanoshell (dashed line) and semishell (solid line) in a PDMS film. Panels C and D are electric field ($\log|E|^2$) profiles (top) and charge distributions (bottom) of a Au semishell at on-resonance excitation wavelengths of (C) 892 and (D) 691 nm.

CONCLUSION

We have successfully fabricated various separated metallic (Ag, Au, Cu, and Al) semishells in PDMS films. The analysis of experimentally resolved and FDTD calculated extinction spectra, with the electric field and surface charge distribution profiles, renders us a clear assignment of the plasmonic modes including dipolar, multipolar, and antibonding modes in metallic semishells. The different material-dependent range of the interband transitions in the metal and resultant damping lead to different plasmonic behaviors of different metallic semishells. Especially, the relatively higher energy onset of the interband transitions in Ag allows more plasmon resonances of Ag semishells near the UV region, which are especially interesting for some optical application in the UV range. The experimental observation of the antibonding mode in the UV region in Ag semishells, supported by a detailed understanding based on the simulation, demonstrates the effectiveness of the plasmon hybridization model as a tool to design and predict the optical properties of metallic nanostructures. The clear understanding of the plasmonic modes of semishells is in aid of the development of new optical applications for semishells. The obtained symmetry-broken semishell nanostructures also have wide potential applications in LSPR biosensing, optical communication, SERS-based molecular detection, and thin film solar cells.

METHODS

Materials. Polydiallyldimethylammonium (PDDA, M_w 100000−200000, 20 wt % in H_2O) was supplied by Sigma Aldrich (Steinheim, Germany). 2-Propanol, acetone, and ethanol (absolute) were bought from Honeywell Specialty Chemicals (Seelze, Germany). Polystyrene (PS) sulfate latex beads (100 nm, 5.4% coefficient of variation, 8.2% solid percent) were purchased from Interfacial Dynamics Corp. (Portland, OR). The PDMS prepolymer (Sylgard 184) and curing agent were obtained from Dow Corning (Wiesbaden, Germany).

Fabrication of Semishells. Prior to use, a glass substrate slide was coated with a 10 nm thick sputtered titanium (Ti) layer. Afterward, the substrate was cleaned for 5 min by subsequently submerging in acetone (45 ± 2 °C) and 2-propanol (60 ± 2 °C), respectively, rinsed well by deionized H_2O, and dried in a nitrogen stream. Then the substrate surface was functionalized by pipetting a 1 mL aqueous solution containing 0.2 wt % PDDA onto the substrate, followed by a careful rinsing with deionized H_2O in order to remove the excess PDDA and drying in a nitrogen stream. Deposition of an aqueous suspension containing 100 nm PS beads (0.2% solid percent), careful rinsing by deionized H_2O, and drying in a nitrogen steam resulted in the glass substrate being covered by uniformly distributed PS beads as a sacrificial mask. A 10−30 nm thick metallic film of Au, Ag, Al, or Cu was sputtered subsequently on top of the PS masks. The next step involved coating the substrate with a PDMS polymer film. The PDMS resin mixed with the curing agent (5:1) was directly casted on the surface of the substrate and a 10 min degassing process was carried out. The polymerization was allowed to continue overnight at 50 °C in a vacuum oven. Finally, after polymerization the PDMS films containing embedded semishells were peeled off the substrate.

Characterization Techniques. SEM images were taken using a Philips XL30 FEG instrument operated at an accelerating voltage of 5 kV. UV−vis spectra were measured using a Shimadzu UV-1601PC spectrophotometer with a spectral bandwidth of 2 nm and a data interval of 0.5 nm. The PDMS film with embedded metallic semishells was placed on a glass slide and the whole slide was oriented perpendicularly to the incident light during the measurement in air. AFM images were acquired in a tapping mode on a Dimension 3100/Nanoscope IV, VEECO, under ambient conditions with the scan rate between 0.4 and 0.5 Hz. Si cantilevers with a force constant between 12 and 103 N/m were used at resonance frequencies between 200 and 400 kHz.

Theoretical methods. Calculated extinction spectra, electric field and surface charge distribution images were obtained from FDTD calculations using the program FDTD Solutions (Lumerical Solutions, Inc., Canada). A metallic semishell embedded in a matrix is illuminated with a total-field scattered-field (TFSF) source, which propagates in the *k* direction. The direction of the electric field *E* is perpendicular to *k* (Figure 1). A perfectly matched layer is used as radiation boundary condition. The simulation region is 600 × 600 × 600 nm^3 with a nonuniform mesh adapted to the structure plus a uniformly meshed region 250 × 250 × 250 nm^3 with a grid size of 3 nm. The whole simulation region is set with a background index of 1 (air) and the PDMS matrix substrate is set with a refractive index of 1.45. We have used the Lumerical's multicoefficient model (MCM)[29] to fit the empirical Ag,[30] Au,[31] Cu,[31] and Al[31] dispersion data. Once the resonance frequencies are determined, on-resonance excitation is used to excite individual modes to examine the corresponding field distribution by using a meshed region of 1 nm grid size. We take models of the metallic semishells with sharp edges in order to simplify the simulations. In contrast to the structures with round edges, we have found that the presence of the sharp features may result in slight shifts of the plasmon resonance bands and obviously more pronounced electric field enhancement. However, we do not observe any noticeable difference with plasmon resonance modes, charge distribution, and other results.

Acknowledgment. P.V.D. acknowledges financial support from the FWO of Flanders. N.V. acknowledges support from the Methusalem funding by the Flemish Government.

Supporting Information Available: A large area AFM topographic image of Au semishells, SEM images of Au semishells fabricated with different ratios of PDMS prepolymer to curing agent, and the calculated extinction spectrum of Al semishells with 20 nm shell thickness in PDMS. This material is available free of charge *via* the Internet at http://pubs.acs.org.

REFERENCES AND NOTES

1. Charnay, C.; Lee, A.; Man, S.; Moran, C. E.; Radloff, C.; Bradley, R. K.; Halas, N. Reduced Symmetry Metallodielectric Nanoparticles: Chemical Synthesis and Plasmonic Properties. *J. Phys. Chem. B* **2003**, *107*, 7327–7333.
2. Mirin, N. A.; Halas, N. J. Light-Bending Nanoparticles. *Nano Lett.* **2009**, *9*, 1255–1259.
3. Srivastava, A. K.; Madhavi, S.; White, T. J.; Ramanujan, R. V. The Processing and Characterization of Magnetic Nanobowls. *Thin Solid Films* **2006**, *505*, 93–96.
4. Liu, J.; Zhu, M.; Zhan, P.; Dong, H.; Dong, Y.; Qu, X.; Nie, Y.; Wang, Z. Morphology−Controllable Fabrication of Ordered Platinum Nanoshells with Reduced Symmetry. *Nanotechnology* **2006**, *17*, 4191–4194.
5. Ye, J.; Van Dorpe, P.; Van Roy, W.; Lodewijks, K.; De Vlaminck, I.; Maes, G.; Borghs, G. Fabrication and Optical Properties of Gold Semishell. *J. Phys. Chem. C* **2009**, *113*, 3110–3115.
6. Ye, J.; Van Dorpe, P.; Van Roy, W.; Borghs, G.; Maes, G. Fabrication, Characterization, and Optical Properties of Gold Nanobowl Submonolayer Structures. *Langmuir* **2009**, *25*, 1822–1827.
7. Farcau, C.; Astilean, S. Probing the Unusual Optical Transmission of Silver Films Deposited on Two-Dimensional Regular Arrays of Polystyrene Microspheres. *J. Opt. A: Pure Appl. Opt.* **2007**, *9*, S345–S349.
8. Landström, L.; Brodoceanu, D.; Bäuerle, D.; Garcia-Vidal, F. J.; Rodrigo, S. G.; Martin-Moreno, L. Extraordinary Transmission Through Metal-Coated Monolayers of Microspheres. *Opt. Express* **2009**, *17*, 761–772.
9. Liu, J.; Maaroof, A. I.; Wieczorek, L.; Cortie, M. B. Fabrication of Hollow Metal "Nanocaps" and Their Red-Shifted Optical Absorption Spectra. *Adv. Mater.* **2005**, *17*, 1276–1281.
10. Liu, J.; Cankurtaran, B.; McCredie, G.; Ford, M. J.; Mieczorek, L.; Cortie, M. Investigation of the Optical Properties of Hollow Aluminium "Nanocaps". *Nanotechnology* **2005**, *16*, 3023–3028.
11. Liu, J.; Cankurtaran, B.; Wieczorek, L.; Ford, M. J.; Cortie, M. Anisotropic Optical Properties of Semitransparent Coating of Gold Nanocaps. *Adv. Funct. Mater.* **2006**, *16*, 1457–1461.
12. Maaroof, A. I.; Cortie, M. B.; Harris, N.; Wieczorek, L. Mie and Bragg Plasmons in Subwavelength Silver Semishells. *Small* **2008**, *4*, 2292–2299.
13. Lu, Y.; Liu, G. L.; Kim, J.; Mejia, Y. X.; Lee, L. P. Nanophotonic Crescent Moon Structures with Sharp Edge for Ultrasensitive Biomolecular Detection by Local Electromagnetic Field Enhancement Effect. *Nano Lett.* **2005**, *5*, 119–124.
14. Prodan, E.; Radloff, C.; Halas, N. J.; Nordlander, P. A Hybridization Model for the Plasmon Response of Complex Nanostructures. *Science* **2003**, *302*, 419–422.
15. Kelf, T. A.; Sugawara, Y.; Cole, R. M.; Baumberg, J. J.; Abdelsalam, M. E.; Cintra, S.; Mahajan, S.; Russell, A. E.; Bartlett, P. N. Localized and Delocalized Plasmons in Metallic Nanovoids. *Phys. Rev. B* **2006**, *74*, 245415/1–12.
16. Jensen, T. R.; Malinsky, M. D.; Haynes, C. L.; Van Duyne, R. P. Nanosphere Lithography: Tunable Localized Surface Plasmon Resonance Spectra of Silver Nanoparticles. *J. Phys. Chem. B* **2000**, *104*, 10549–10556.
17. Baia, L.; Baia, M.; Popp, J.; Astilean, S. Gold Films Deposited over Regular Arrays of Polystyrene Nanospheres as Highly Effective SERS Substrates from Visible to NIR. *J. Phys. Chem. B* **2006**, *110*, 23982–23986.
18. Wang, H.; Fu, K.; Drezek, R. A.; Halas, N. J. Light Scattering from Spherical Plasmonic Nanoantennas: Effects of Nanoscale Roughness. *Appl. Phys. B: Laser Opt.* **2006**, *84*, 191–195.
19. Wang, H.; Tam, F.; Grady, N. K.; Halas, N. J. Cu Nanoshells: Effects of Interband Transitions on the Nanoparticle Plasmon Resonance. *J. Phys. Chem. B* **2005**, *109*, 18218–18222.
20. Johnson, P. B.; Christy, R. W. Optical Constants of the Noble Metals. *Phys. Rev. B* **1972**, *6*, 4370–4379.
21. Wang, H.; Goodrich, G. P.; Tam, F.; Oubre, C.; Nordlander, P.; Halas, N. J. Controlled Texturing Modifies the Surface Topography and Plasmonic Properties of Au Nanoshells. *J. Phys. Chem. B* **2005**, *109*, 11083–11087.

22. Lee, K.-H.; Chang, K. J. First-Principle Study of the Optical Properties and the Dielectric Response of Al. *Phys. Rev. B* **1994**, *49*, 2362–2367.
23. Ehrenreich, H.; Philipp, H. R.; Segall, B. Optical Properties of Aluminum. *Phys. Rev.* **1963**, *132*, 1918–1928.
24. Langhammer, C.; Schwind, M.; Kasemo, B.; Zorí, I. Localized Surface Plasmon Resonances in Aluminum Nanodisks. *Nano Lett.* **2008**, *8*, 1461–1471.
25. Park, T.; Nordlander, P. On the Nature of the Bonding and Antibonding Metallic Film and Nanoshell Plasmons. *Chem. Phys. Lett.* **2009**, *472*, 228–231.
26. Ye, J.; Van Dorpe, P.; Lagae, L.; Maes, G.; Borghs, G. Observation of Plasmonic Dipolar Anti-Bonding Mode in Silver Nanoring Structures. *Nanotechnology* **2009**, *20*, 465203/1–6.
27. Hao, F.; Larrson, E. M.; Ali, T. A.; Sutherland, D. S.; Nordlander, P. Shedding Light on Dark Plasmons in Gold Nanorings. *Chem. Phys. Lett.* **2008**, *458*, 262–266.
28. Ye, J.; Liesbet, L.; Maes, G.; Borghs, G.; Van Dorpe, P. Symmetry Breaking Induced Optical Properties of Gold Open Shell Nanostructures. *Opt. Express* **2009**, *17*, 23765–23771.
29. Lumerical. http://www.lumerical.com. Accessed April 20, 2009.
30. Palik, E. D., Ed. *Handbook of Optical Constant of Solids*; Academic Press: Orlando, FL, 1985.
31. Lide, D. R., Ed. *CRC Handbook of Chemistry and Physics,* 3rd electronic ed.; CRC Press: Boca Raton, FL, 2000.